Agreement between Analytical Theory and Molecular Dynamics Simulation for Adsorption and Diffusion in Crystalline Nanoporous Materials

Mithun Kamat, Weijing Dang, and David Keffer*

Department of Chemical Engineering, University of Tennessee, 1512 Middle Drive, Knoxville, Tennessee 37996-2200

Received: June 19, 2003; In Final Form: October 14, 2003

Analytical theories for lattice adsorption and diffusion recently published are tested with molecular dynamics (MD) simulations. Our analytical theories are generalized and can be applied to various small molecules in different nanoporous structures such as zeolites and molecular sieves. In this work, we validate our theory by comparing the results with those predicted by simulations. We study the behavior of methane in zeolite Na-Y. Specifically, the MD simulations are conducted to obtain the interaction energies and self-diffusion coefficients at five different temperatures and loadings. While the lattice adsorption theory incorporates minimum parameters to obtain the thermodynamic properties, the diffusion component of the theory incorporates no adjustable parameters. Our theory is in very good qualitative agreement with the simulations. Overall, reasonably good quantitative agreement is found between the theory and simulations. Our theory studies the effect of temperature and density on the adsorption and diffusion of methane in Na-Y. Our theory requires approximately only a minute to obtain the results, as compared with the tens of CPU hours required for simulations.

1. Introduction

A significant body of literature has been devoted to investigating the phenomenon of adsorption and diffusion in nanoporous materials.[1−92] These phenomenon are of great scientific interest due to their increasingly wide range of applicability in separation and catalysis processes.[91,92] Molecular level simulations have established that competing entropic and energetic effects play an important role in the placement of adsorbates within nanoporous materials. It has been determined that both the adsorbate−adsorbate and adsorbate−pore interactions within the nanoporous material dictate the extent of adsorption. However, some areas of uncertainty still persist. For instance, literature suggests that different systems evolving from the vast range of nanoporous materials, such as molecular sieves, zeolites, and MCM-type materials, often give contradictory results for different fluids, for example, the diffusivity of methane varies differently for different adsorbents as a function of loading and temperature.[93−95] Also, the industry is constantly exploring the applicability of new nanoporous materials as effective adsorbents. The problem is that the computationally expensive simulations are often seen as inefficient platforms to produce quick results. These problems can be overcome by the development of a quick, predictive theory that would successfully yield intelligent first estimates, which can be later confirmed by simulations, and increase the understanding of the behavior of fluids in nanoporous materials. The theory would provide a unified approach to highlight the physical mechanisms occurring at the molecular level, which would elucidate such seemingly contradictory results.

There have been previous worthwhile attempts to develop analytical theories of adsorption and diffusion based on lattice models. Of note in this connection is the work of Saravanan et al. who developed an analytical theory of diffusion for benzene in Na-Y.[87−90] Van Tassel et al. introduced a lattice model for the adsorption of small molecules in zeolite NaA.[16,17] Snurr et al. presented a lattice model for adsorption of benzene in silicalite.[38] In our previous work, we presented unifying analytical theories for adsorption and diffusion of fluids in nanoporous materials such as molecular sieves and zeolites.[1,2] We suggested that our analytical theory is more easily generalizable to various solid−fluid interacting systems than the previously attempted models. Also, our theory incorporates a minimum number of parameters, which makes it easily accessible for broader usage. Having said that, our second step is to validate these theories with the simulations.

This paper intends to compare the results of our analytical theories for adsorption and diffusion with molecular dynamics simulations for a specific solid−fluid contacting system, namely, methane in Na-Y.

Zeolite Na-Y has a three-dimensional channel system consisting of cavities separated by 12-membered oxygen rings. It has nearly 50% of the volume of the crystal available for adsorption with a Si/Al ratio of 1.3. We have mentioned previously how the diffusivity of methane shows different trends for different adsorbents. It is seen that the diffusivity increases with loading for one adsorbent, decreases with loading for a second, and shows a minimum for a third adsorbent.[93−95] Though simulations reveal these trends and explain them to a reasonable extent, our theory investigates the fundamental molecular level mechanisms to understand the underlying physical mechanisms.

The remainder of this paper is organized as follows. Section 2 provides a brief review of our analytical theories of adsorption and diffusion. Also included is a discussion on the functional form of the external potential. Section 3 discusses the MD simulation methodology and convergence criteria. Also, the numerical optimization routine for convergence parameters is discussed. Section 4 presents the results from theory and simulation for methane in Na-Y and the comparison between

* To whom correspondence should be addressed. E-mail: dkeffer@utk.edu.

10.1021/jp035745g CCC: $27.50
Published on Web 12/09/2003

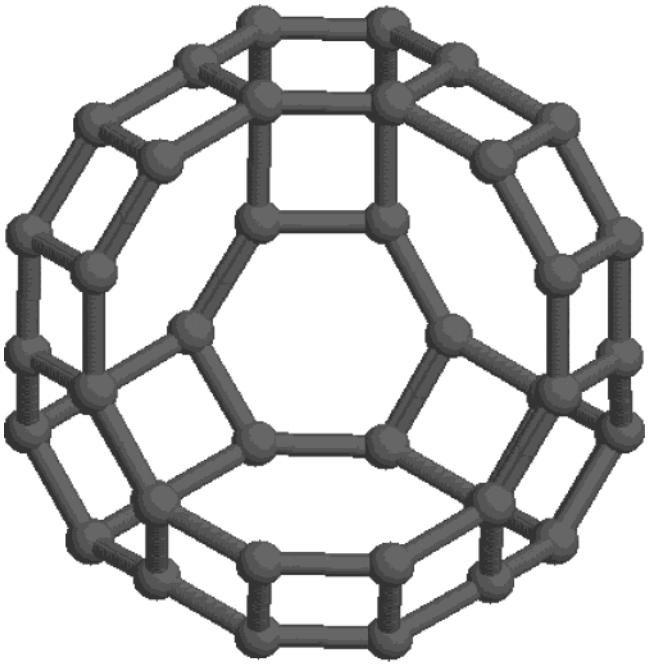

Figure 1. Schematic of the zeolite Na-Y cage structure.

the two. Finally, section 5 presents the conclusions and findings from this work.

2. Theory

A. Review of the Lattice Adsorption Theory. Our predictive theory of adsorption in nanoscopically confined pore spaces is a lattice model.[1] We use standard statistical mechanics to develop the partition functions for the adsorbate molecules. The partition functions are used to obtain the desired thermodynamic and transport properties. There are four factors that determine the nanoporous environment: (i) adsorption site volume, (ii) adsorption site energetic well depth, (iii) lattice connectivity, and (iv) lattice spacing. In other words, these four parameters characterize the lattice.

The lattice model uses a generalization of the standard quasi-chemical approximation to account for the adsorbate−adsorbate interactions. The quasi-chemical approximation is the simplest approximation that will still allow for adsorbate clustering within the pore.[96] The standard quasi-chemical theory is limited to a lattice consisting of just one type of site. But most of the zeolites and molecular sieves are found to have more than one type of site. The standard quasi-chemical approximation cannot model these complex lattices. However, we expand upon the quasi-chemical theory and use it to describe these lattices because the lattice sites are still localized.

Let's assume an arbitrary lattice with two types of sites, $N_T = 2$. This lattice is described by a connectivity matrix, $\underline{\underline{c}}$, where

$$\underline{\underline{c}} = \begin{bmatrix} c_{11} & c_{12} \\ c_{21} & c_{22} \end{bmatrix} \tag{1}$$

where each of these elements, c_{ij}, describe the number of sites of type j connected to a site of type i. Specifying the connectivity in this way specifies the relative number of sites of types 1 and 2, M_1 and M_2.

As an example consider the lattice schematic in Figure 1. In this case,

$$\underline{\underline{c}} = \begin{bmatrix} 0 & 3 \\ 2 & 0 \end{bmatrix}.$$

The number of sites of type 1 and 2 must obey the relations

$$\sum_{i=1}^{N_T} M_i = M \tag{2.1}$$

and a neighbor balance

$$c_{12}M_1 = c_{21}M_2 \tag{2.2}$$

which determines M_1 and M_2 to be

$$M_1 = \frac{c_{21}}{c_{12}+c_{21}}M \quad \text{and} \quad M_2 = \frac{c_{12}}{c_{12}+c_{21}}M \tag{3}$$

The separation between nearest-neighbor sites is given by a matrix of distances, $\underline{\underline{\ell}}$. The sites have a well depth of $U_{AP,i}(x)$, which is the potential energy due to adsorbate−pore interactions. $U_{AP,i}(x)$ is a function of x, the occupancy of the site, and of site type i. The sites have volume, $V_{S,i}$. The four parameters—$\underline{\underline{c}}$, $\underline{\underline{\ell}}$, $U_{AP}(x)$, and V_S—completely characterize the lattice.

We use an arbitrary pairwise potential to model the adsorbate−adsorbate interactions, evaluating it at $\underline{\underline{\ell}}$ to obtain $\underline{\underline{\underline{\underline{\mathbf{w}_x}}}}$.

The partition function has three factors, a configurational degeneracy, intrasite partition function, and intersite interaction energy:

$$Q(N,M,T) = \sum_{\text{configurations}} g(N,M)\prod_{i=1}^{N_T}\left[\prod_{x=1}^{m_{s,i}} q_i(x,T)^{x n_{s,i}(x)}\right] \exp\left[-\sum_{i=1}^{N_T}\sum_{j\geq i}^{N_T}\sum_{x=1}^{m_{s,i}}\sum_{y^*}^{m_{s,i}} N_{ij,xy}\frac{\mathbf{w}_x}{kT}\frac{\mathbf{w}_x}{kT}\right] \tag{4}$$

There are two points to be noted here. First, the summation includes only combinations of i and j that have nearest neighbors (i.e., $c_{ij} \neq 0$). Second, the index y^* varies. If the sites are the same ($i = j$), then $y^* \geq x$. If the sites are different ($i \neq j$), $y^* \geq 1$. In this way, we avoid double counting. Also, the maximum occupancy of a site of type i is $m_{s,i}$, the intrasite partition function is $q_i(x,T)$, and the number of sites with occupancy x, $n_{s,i}(x)$, is defined for each site of type i. The number of neighbors, $N_{ij,xy}$, designates the number of neighbors between sites of type i with occupancy x and sites of type j with occupancy y.

We extend the quasi-chemical approximation to determine the general configurational degeneracy as

$$g(N,M) = \left[\prod_{\substack{i=1 \\ j\neq i}}^{N_T}\left(\frac{M_i!}{\prod_{x=0}^{m_{s,i}} n_s(x)!}\right)^{1-c_{ij}}\right]\left[\frac{(c_{12}M_1)!}{\prod_{x=0}^{m_{s,i}}\prod_{y=0}^{m_{s,j}} N_{ij,xy}!}\right] \tag{5}$$

This general form would be altered to meet particular forms of the connectivity matrix. We consider the case of the connectivity matrix given in eq 1.

Determining the partition function would be a case of solving a set of equations for the various unknowns, as has been outlined before.[1] These equations can be generated from the following relations: (1) site balances; (2) adsorbate balances; (3) symmetry relations for the number of neighbors; (4) a balance on the number of neighbors. We minimize the partition function with

respect to these unknowns to obtain the remaining equations. Thus, we have a system of nonlinear algebraic equations with an equal set of unknowns. It was shown in our previous paper on lattice adsorption theory that an analytical solution was obtained only for the single case, $N_t = 2$, $m_{s,1} = 1$, $m_{s,2} = 1$, and $\mathbf{w} = 0$.[1] For all other cases, we employed a numerical solution.

Once the variables are known, we can formulate the partition function and solve for any thermodynamic variables of interest. For example, the Helmholtz free energy, A, given by

$$A = -kT \ln Q \tag{6}$$

can be obtained by solving for numerical values of the unknowns and substituting them into the partition function. Similarly, we can obtain analytical expressions for the total energy, E (kinetic and potential), and the entropy, S, from

$$E = kT^2\left(\frac{\partial \ln Q}{\partial T}\right)_{N,M\{\text{unknowns}\}} \tag{7}$$

and

$$S = -A + E/T \tag{8}$$

B. Review of the Lattice Diffusion Theory. The diffusion component of our lattice theory is based on the assumption that lattice diffusion is an activated process with Arrhenius temperature dependence.[2] For instance, an activated process requires motion from a site of type 1 to an adjacent site of type 1 to pass through a site of type 2. Sites of type 2 are considered "the activated state" sites. Similarly, sites of type 1 are the activated sites when allowing motion between two adjacent sites of type 2. The activation energy is simply the difference in the potential energy for an adsorbate in a site of type 1 and type 2. It is important to bear in mind the fact that the activation energy has a strong dependence on the site occupancy and the pore well depth. We assume a functional form of the diffusion coefficient as

$$D(n,m,T) = \sum_{i=1}^{N_t}\sum_{x=0}^{m_{s,i}} \frac{x n_{s,i}(x)}{n} \frac{1}{c_{ij}} \sum_{j=1}^{N_t} c_{ij} \sum_{y=0}^{m_{s,j}} \frac{N_{ij}(x,y)}{\sum_{z=0}^{m_{s,j}} N_{ij}(x,z)} D_{ij}(x,y,T) \tag{9}$$

Some of the unknowns in eq 9 can be obtained from our lattice adsorption theory. Also, the above equation includes weighting functions to account for the various factors, such as site occupancy and lattice connectivity, affecting a jump of an adsorbate molecule from site of type 1 to site of type 2. The only factor required to obtain the average diffusivity, then, is the local diffusivity, $D_{ij}(x,y,T)$. This function has the standard activated form:

$$D_{ij}(x,y,T) = D_{0,ij}(x)\, e^{[\Delta E_{ji}^*(y+1,x,T)]/(kT)}\, h_{ij}(x,y) \tag{10}$$

where $\Delta E_{ji}^*(y+1,x,T)$ is an activation barrier to motion, which is defined as

$$\Delta E_{ij}(x,y,T) = \begin{cases} \Delta E_{ij}(x,y,T) & \text{if } \Delta E_{ij}(x,y,T) > 0 \\ 0 & \text{if } \Delta E_{ij}(x,y,T) \le 0 \end{cases} \tag{11}$$

This modified barrier allows activated motion to occur, when the change in total energy is positive, and allows the move to occur freely, when the change is zero or negative.

The weighting function, $h_{ij}(x,y)$, eliminates impossible moves, such as a hop from an origin site that is empty or a hop to a destination site that is already at maximum occupancy.

$$h_{ij}(x,y,T) = \begin{cases} 0 & \text{if } x = 0 \\ 0 & \text{if } y = m_{s,j} \\ 1 & \text{otherwise} \end{cases} \tag{12}$$

Our analytical theory of adsorption delivers $E_i(x,T)$ from which we can obtain the difference needed in eq 11.

$$\Delta E_{ji}(y+1,x,T) = E_i(x,T) - E_j(y+1,T) \tag{13}$$

Furthermore, the prefactor $D_{0,ij}(x)$ in eq 10 provides the frequency with which moves are attempted and the mean-square displacement of a successful move.

$$D_{0,ij}(x,y) = \frac{\omega_i(x) \lambda_{ij}^2}{2} \tag{14}$$

The frequency of attempted hops of an adsorbate in a site of type i with occupancy x, $\omega_i(x)$, is given by

$$\omega_i(x) = \frac{\upsilon}{D_{s,\text{eff},i}(x)} \tag{15}$$

The frequency is the average velocity over the characteristic dimension of the site. The velocity, υ, is given by

$$\upsilon = \sqrt{\frac{3kT}{m_a}} \tag{16}$$

where m_a is the molecular mass of the adsorbate. The velocity is the same for all adsorbates regardless of the type of site in which they reside or its occupancy. The effective diameter of the site, $D_{s,\text{eff},i}(x)$, assumes that the sites and the adsorbate are spherical and is given by

$$D_{s,\text{eff},i}(x) = \sqrt[3]{\frac{6}{\pi} V_{s,\text{eff},i}(x)} = \sqrt[3]{\frac{6}{\pi}(V_{s,i} - xV_a)} \tag{17}$$

where $V_{s,\text{eff},i}(x)$ is the effective volume of a site of type i with occupancy x, $V_{s,i}$ is the empty volume, and V_a is the volume of the adsorbate.

C. Functional Form of the External Potential. Our lattice theory can be generalized to any arbitrary functional form of the external potential, $\overline{\overline{U_{AP}}}$—the adsorbate−pore interaction energy. Here, we select a slightly different functional form. Unlike our previous assumption,[1] the adsorbate−pore (AP) interaction energy could have a strong dependence on temperature in addition to the site occupancy. In other words, the AP interaction energy, $\overline{\overline{U_{AP}}}$, is now a function of site occupancy and temperature.

The functional form of the local AP interaction energy assumes spherical sites and adsorbates and is a parabolic function of the site radius, r. Let's designate the local AP interaction energy as $U_{AP,i}(r,x)$. Thus, the interaction energy between the adsorbate and the walls of the pore is a function of (i) energetic well depth, (ii) site occupancy, and (iii) pore radius, given by

$$U_{AP,i}(r,x) = U_{AP,i}(x) + U_{APc,i} r_i^2 \tag{18}$$

The pore radius r_i can be evaluated from the site volume:

$$V_{s,i} = \frac{4}{3}\pi r_i^3 \tag{19}$$

$U_{AP,i}(x)$ is the pore well depth, which is a function of the site occupancy. We use a Boltzmann distribution to calculate the average AP interaction energy for a given temperature T, given by

$$U_{AP,i}(r,x,T) = \frac{\int_{r=0}^{r=r_{max}} U_{AP,i}(r,x)\, e^{(-U_{AP,i}(r,x)/(k_b T))}\, r_i^2\, dr}{\int_{r=0}^{r=r_{max}} e^{(-U_{AP,i}(r,x)/(k_b T))}\, r_i^2\, dr} \tag{20}$$

where $e^{(-U_{AP,i}(r,x)/(k_b T))}$ is the Boltzmann weighting distribution. Solving the integral, we get

$$U_{AP,i}(r,x,T) = U_{AP,i}(r,x) + \frac{3}{2}k_b T + \frac{U_{APc,i} r_{max}^2}{1 - \frac{1}{2}\sqrt{\pi}\frac{\operatorname{erf}\left[r_{max}\sqrt{\frac{U_{APc,i}}{k_b T}}\right]}{r_{max}\sqrt{\frac{U_{APc,i}}{k_b T}}\, e^{[r_{max}^2 U_{APc,i}/(k_b T)]}}} \tag{21}$$

Notice in eq 18 that we use a constant term, $U_{APc,i}$, for each type of site. Overall, the net result of including the temperature dependence of the AP interaction energy is that we have one additional fitting parameter, $U_{APc,i}$, for each type of lattice site.

3. Simulations and Numerical Methods

Simulation Methodology. We perform molecular dynamics (MD) simulations in the microcanonical ensemble, that is, keeping the number of adsorbates, N, the volume, V, and the total energy, E, fixed.[97,98] We use the Lennard-Jones 6-12 potential to model the adsorbate−adsorbate interactions:

$$U_{AA} = \sum_{i=1}^{N-1}\sum_{j-i+1}^{N} U_{ij} = \sum_{i=1}^{N-1}\sum_{j=1+1}^{N} 4\epsilon_{ij}\left[\left(\frac{\sigma_{ij}}{r_{ij}}\right)^{12} - \left(\frac{\sigma_{ij}}{r_{ij}}\right)^{6}\right] \tag{22}$$

where the potential parameters ϵ and σ for methane are obtained from ref 99 and are given in Table 1. For the adsorbate−pore interactions, we use atomic positions for the oxygen atoms in zeolite Na-Y. Only oxygen atoms contribute significantly to the external potential,[85] permitting us to ignore the Si and Al. We ignore the charge on the oxygen. We use the Lennard Jones 6-12 potential to model the adsorbate−pore interactions. The parameters are listed in Table 1.

We simulate 128−512 atoms per unit cell, depending upon the density. For low density, we use 128 atoms, and we increase the number for higher densities. A cutoff distance, r_{cut}, of 15 Å and a neighbor distance, r_{nbr}, of 18 Å is employed. We use a time step of 2 fs, and carry out 10 000 equilibration steps and 100 000 data production steps. The numerical solution technique used is the 5th order gear predictor corrector.[100,101] Periodic boundary conditions and the standard minimum image convention are employed along the boundaries of the unit cell of Na-Y.

The self-diffusivities are calculated using the Einstein relation,[97] which relates the self-diffusion coefficient to the mean-square displacement of a particle as a function of observation time, given by

$$D = \frac{1}{2d}\lim_{\Delta t\to\infty}\frac{\langle[\underline{r}(t_0+\Delta t) - \underline{r}(t_0)]^2\rangle}{\Delta t} \tag{23}$$

where D is the self-diffusion coefficient and d is the dimensionality of the system. The numerator of eq 23 is the mean-square displacement.

TABLE 1: Potential Parameters

	ϵ_{ij}/k {K}	σ_{ij} {Å}
methane−methane	137	3.882
methane−oxygen	141	3.08
oxygen−oxygen		3.04

TABLE 2: Simulation Results for Methane in Zeolite Na-Y

density adsorbate/site	E_{AA} {K}	E_{AP} {K}	E_{TOT} {K}	diffusivity {m²/s}	temp {K}
0.0	0.00×10^{0}	-8.62×10^{2}	-7.12×10^{2}	7.80×10^{-9}	100
0.05	-3.43×10^{1}	-8.55×10^{2}	-7.41×10^{2}	6.36×10^{-9}	
0.2	-1.30×10^{2}	-8.40×10^{2}	-8.21×10^{2}	6.29×10^{-9}	
0.4	-2.49×10^{2}	-8.26×10^{2}	-9.29×10^{2}	3.75×10^{-9}	
0.8	-4.66×10^{2}	-8.04×10^{2}	-1.12×103	2.27×10^{-9}	
0.0	0.00×10^{0}	-7.61×10^{2}	-4.61×10^{2}	2.28×10^{-8}	200
0.05	-2.82×10^{1}	-6.79×10^{2}	-4.07×10^{2}	2.50×10^{-8}	
0.2	-1.08×10^{2}	-6.79×10^{2}	-4.90×10^{2}	1.87×10^{-8}	
0.4	-2.12×10^{2}	-6.82×10^{2}	-5.91×10^{2}	1.25×10^{-8}	
0.8	-4.29×10^{2}	-6.92×10^{2}	-8.23×10^{2}	6.06×10^{-9}	
0.0	0.00×10^{0}	-6.97×10^{2}	-2.50×10^{2}	3.20×10^{-8}	298
0.05	-2.51×10^{1}	-6.06×10^{2}	-1.84×10^{2}	3.70×10^{-8}	
0.2	-1.01×10^{2}	-6.13×10^{2}	-2.66×10^{2}	3.06×10^{-8}	
0.4	-1.98×10^{2}	-6.22×10^{2}	-3.71×10^{2}	1.85×10^{-8}	
0.8	-4.02×10^{2}	-6.45×10^{2}	-5.96×10^{2}	8.73×10^{-9}	
0.00	0.00×10^{0}	-6.34×10^{2}	-3.38×10^{1}	4.26×10^{-8}	400
0.05	-2.35×10^{1}	-5.64×10^{2}	1.19×10^{1}	5.12×10^{-8}	
0.2	-9.27×10^{1}	-5.76×10^{2}	-6.85×10^{1}	3.86×10^{-8}	
0.4	-1.87×10^{2}	-5.87×10^{2}	-1.75×10^{2}	2.56×10^{-8}	
0.8	-3.70×10^{2}	-6.13×10^{2}	-3.85×10^{2}	1.22×10^{-8}	
0.00	0.00×10^{0}	-5.83×10^{2}	1.67×10^{2}	6.01×10^{-8}	500
0.05	-2.19×10^{1}	-5.42×10^{2}	1.86×10^{2}	6.14×10^{-8}	
0.2	-8.69×10^{1}	-5.50×10^{2}	1.13×10^{2}	4.39×10^{-8}	
0.4	-1.75×10^{2}	-5.64×10^{2}	1.12×10^{1}	3.12×10^{-8}	
0.8	-3.37×10^{2}	-5.90×10^{2}	-1.77×10^{2}	1.36×10^{-8}	

Numerical Methods. This section describes the numerical optimization routine employed to conduct the parameter fitting for the lattice. We optimize the parameters U_{AP}, U_{APc}, and V_s. U_{AP} is the pore well depth, V_s is the site volume, and U_{APc} is a vector of two constants that are included because of the modification of our lattice theory as discussed in the previous section. The lattice parameters, $\underline{\mathbf{c}}$ and $\underline{\ell}$, are not fitted because they are easily available from the information about the lattice dimensions.

The objective function is the error between the results predicted by our theory and simulation for the adsorbate−pore (AP) interaction energy. We optimized the AP interaction energy because we suspect that it is physically the most significant property of interest.

The objective function is given by

$$f = \sum_{i=1}^{n}\frac{X_i^{simulation} - X_i^{theory}}{X_i^{simulation}} \tag{24}$$

where X denotes the AP interaction energy and the summation encompasses all of the data points available from simulations. We employ Nelder and Mead's downhill simplex method to minimize the objective function.[102] The downhill simplex

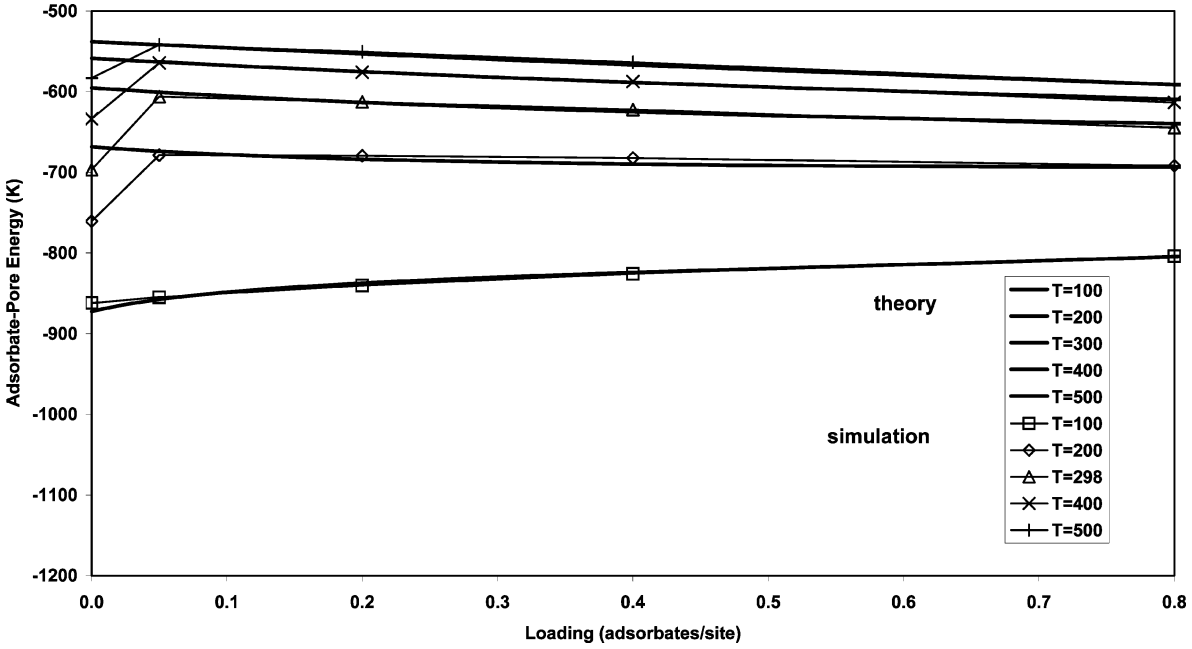

Figure 2. Adsorbate−pore interaction energy as a function of fractional occupancy.

TABLE 3: Lattice Parameters for $N_T = 2$, $m_s = [1\ 2]$

$\underline{\underline{c}}$	$\underline{\underline{l}}$ (Å)	V_S (Å^3)	$\underline{\underline{U_{AP}}}$ (K)	U_{APc} (K)
$\begin{bmatrix} 0 & 3 \\ 2 & 0 \end{bmatrix}$	$\begin{bmatrix} - & 4.304 \\ 4.304 & - \end{bmatrix}$	[35.82,61.87]	$\begin{bmatrix} -1114.826 & -1104.026 \\ -817.515 & -806.715 \end{bmatrix}$	[689.1 635.4]

method is chosen because of its simplicity and robustness. However, the method suffers from a drawback that it depends heavily on the goodness of the initial guesses. A poor initial guess would result in the code converging to a local minimum. We run the code with numerous initial guesses to overcome this limitation and thus ensure that it searches the entire domain of convergence values to decisively locate the global minimum. It is worth mentioning here that the entire optimization routine takes only a few minutes on a desktop PC to converge to the solution. The optimized lattice parameters are listed in Table 2.

4. Results and Discussion

The molecular dynamics (MD) simulations were employed to determine the adsorbate-pore (AP) interaction energy, adsorbate−adsorbate (AA) interaction energy, total energy, and diffusivity. Simulations were conducted at five temperatures and loadings. The simulations took approximately 200 h on the 16-node super computing facility at the University of Tennessee. The simulation results are reported in Table 2. In this section, we present plots to test the results predicted by our theory against these simulations. The theory generated the results in approximately a minute on a standard desktop PC. Both theory and the simulation methodology have been discussed in previous sections.

We study the behavior of single-component methane in Na-Y. Na-Y has roughly spherical nanopores tetrahedrally connected by 12-ring windows (See Figure 1). There are 10 adsorption sites in a cage of Na-Y. Six of them are located octahedrally, one in front of each of the central 4-rings and the other four are located tetrahedrally, one in front of each of the 6-rings. Simulations have previously shown that the adsorption lattice of Na-Y is comprised of two types of localized adsorption sites.[31] The sites differ in the relative accessible pore volume (site volume and occupancy) and the energetic well depth. The numerical values of the lattice parameters are obtained by conducting an optimization (see section 3). The values are reported in Table 3. It is seen that the sites of type 2 are larger and energetically more shallow than the sites of type 1. We mentioned earlier that simulations have shown that the two types of sites have different maximum occupancies. We found that the 2-12 lattice configuration (lattice of two types of sites with sites of type 1 having a maximum occupancy of 1 and sites of type 2 having a maximum occupancy of 2) provided a better fit than the 2-21 case. We hence model the Na-Y sorption lattice as a 2-12 case in our lattice adsorption theory. Also, the sites are connected to each other by a connectivity of

$$c = \begin{bmatrix} 0 & 3 \\ 2 & 0 \end{bmatrix}$$

that is, a site of type 1 is connected to 3 sites of type 2 and a site of type 2 is connected to two sites of type 1.[31] Thus 40% of the total sites are of type 1 and 60% are of type 2.

Figure 2 plots the adsorbate−pore (AP) interaction energy as a function of adsorbate loading for five different temperatures. The AP interaction energy, U_{AP}, is the energetic contribution of the CH_4−O interactions to the total energy. Although Gupta et al. experimentally achieved a maximum adsorbate loading of 18 adsorbates/cage under high-pressure conditions, they report an average density of 10 adsorbates/cage of Na-Y.[31] Correspondingly, we conduct simulations only up through a maximum loading of 0.8 adsorbates/site or 8 adsorbates/cage. Theoretically, however, the 2-12 lattice has 40% of type 1 sites with a maximum occupancy of 1 and 60% of type 2 sites with a maximum occupancy of 2. In other words, the maximum adsorbate loading is $0.4 \times 1 + 0.6 \times 2 = 1.6$ adsorbates/site

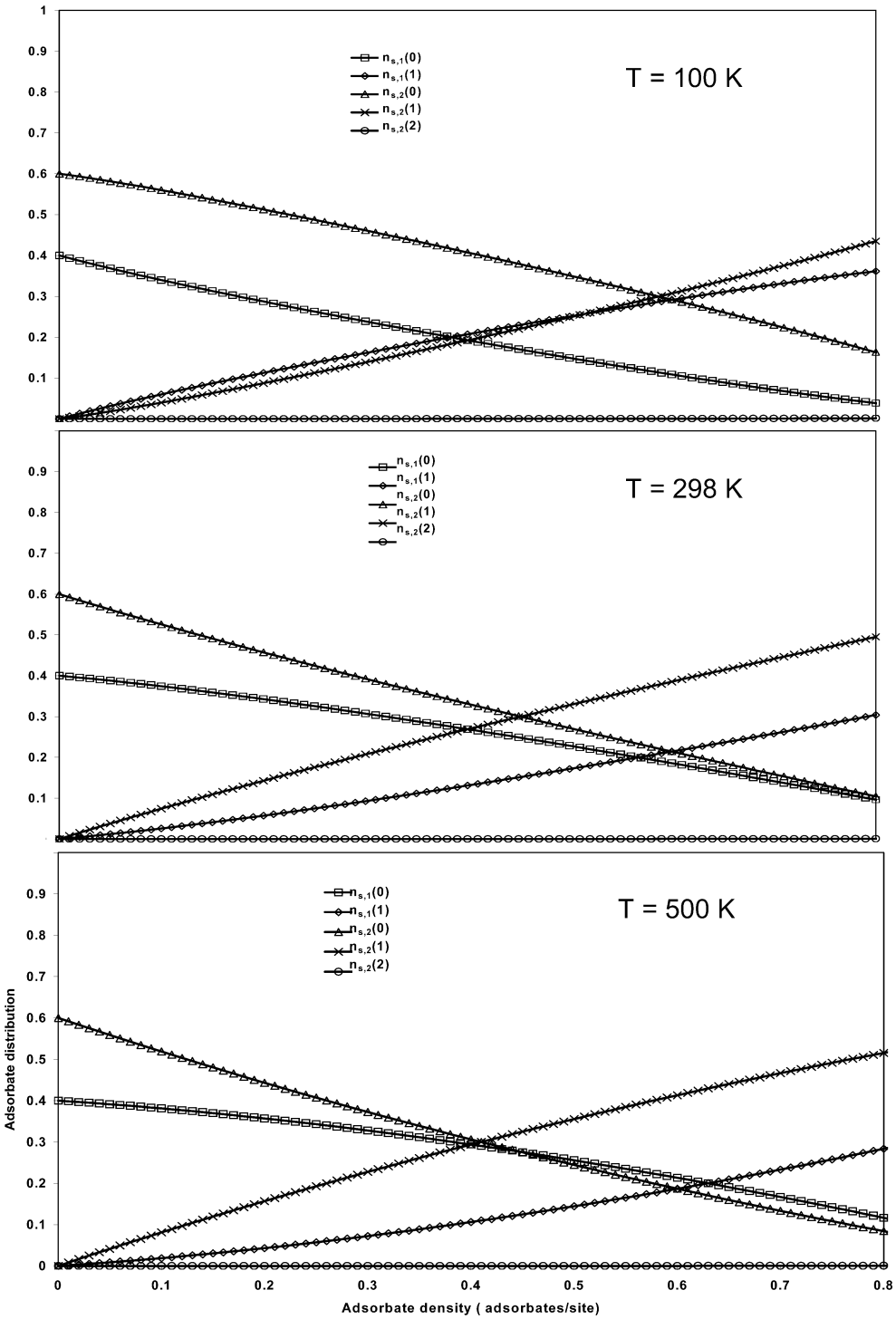

Figure 3. Adsorbate distribution versus adsorbate density.

or 16 adsorbates/cage. Although not shown, our theory can report the interaction energies up through the maximum possible loading of 1.6 adsorbates/site, corresponding to 16 adsorbates/cage.

Figure 2 reveals a very good agreement between the theory and simulations for the AP interaction energy. Our theory and simulation results lie within an average error of 2.3%, which is indicative of the good quantitative agreement between the two. At all loadings, the AP interaction energy increases with an increase in temperature for both theory and simulation. We discussed in section 2 that the AP interaction energy is a function of the site occupancy and temperature. As temperature increases, an adsorbed molecule explores less energetically favorable positions within the site, which increases the AP interaction energy.

The loading dependence of the AP interaction energy is different at different temperatures. At low temperatures, the AP interaction energy monotonically increases with loading. At higher temperatures, the AP interaction energy generally decreases with loading. (Anomalous behavior at infinite dilution will be addressed.) Both theory and simulations predict the nonmonotonic behavior of the AP interaction energy with density and temperature. To understand this behavior, we plot in Figure 3 the adsorbate distribution as a function of loading

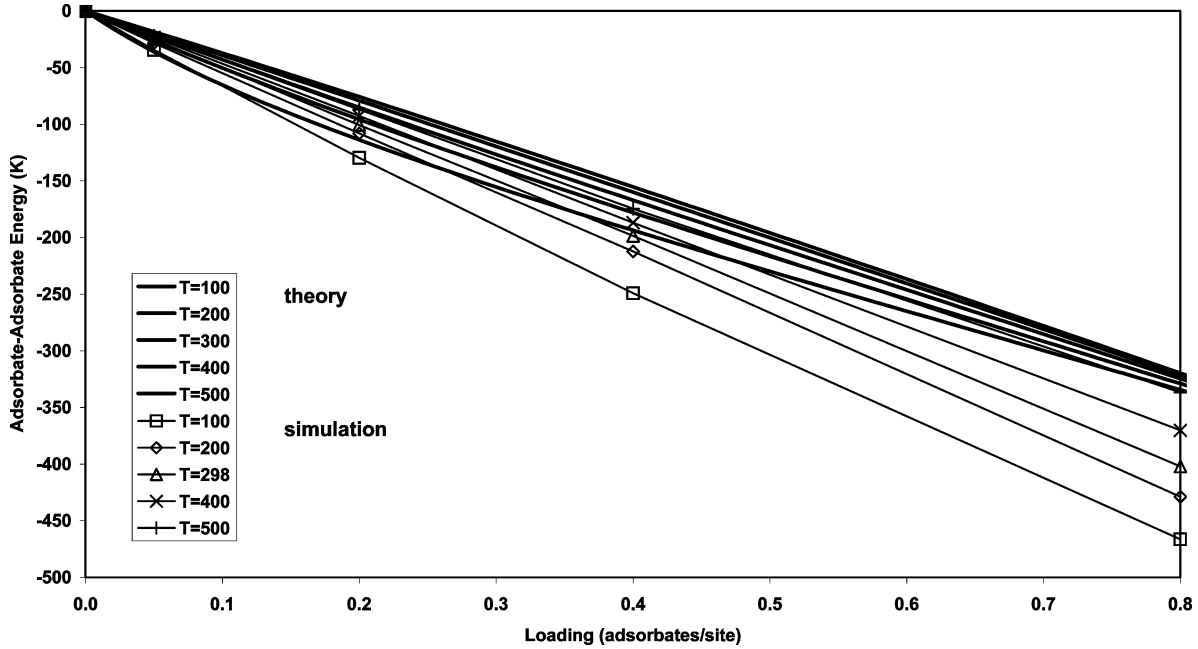

Figure 4. Adsorbate−adsorbate interaction energy as a function of fractional occupancy.

at three different temperatures. An immediate observation here is that the number of sites of type 2 with two adsorbates, $n_{s,2}(2)$, is negligible at all loadings considered. In other words, none of the sites of type 2 are doubly occupied. We see that at higher temperatures, $n_{s,1}(1)$ assumes higher values than $n_{s,1}(1)$ at all loadings up to 0.8 adsorbates/site. In other words, at higher temperatures, a higher number of adsorbates are filled in the sites of type 2 than in the type 1 sites. There is an entropic advantage to placing the molecules in the larger (but energetically shallower) sites of type 2. The combined entropic and energetic effects cause an increase in the number of AP interactions with increasing loading, which results in a decrease of the AP interaction energy. Hence, we see in Figure 2 that the AP interaction energy decreases with loading at higher temperatures. In contrast, at low temperatures, a high number of molecules are adsorbed in the smaller (but energetically deeper) sites of type 1, which results in a decrease in the AP interactions with loading. Correspondingly, we see in Figure 2 that the AP interaction energy increases with loading at low temperatures.

We notice that our theory and simulations do not agree at infinite dilution. At higher temperatures, the simulations show a steep increase in the AP interaction energy at infinite dilution. Our theory does not predict this behavior. We suspect that there is a subtle cross-correlation between the placement of the adsorbate within the sites and the transition from infinite dilution (no neighbors) to low density (few neighbors), which our model does not capture.

Figure 4 plots the adsorbate−adsorbate (AA) interaction energy as a function of loading for five temperatures. The AA interaction energy, U_{AA}, is the energetic contribution of the CH_4-CH_4 interactions to the total energy. It is important to note that the AA interactions occur between the molecules adsorbed in neighboring sites, as well as within sites (2-12 case has doubly occupied sites of type 2). We notice that the theory is qualitatively in agreement with the simulations. Both theory and simulations show that at all temperatures, the AA interaction energy decreases with loading. At all temperatures, the adsorbate−adsorbate interactions increase as loading increases. The density dependence of the AA interactions and correspondingly the AA interaction energy arises from the fact that both the intrasite and the intersite partition functions have a high loading functionality.

Our theory and simulations also observe the same temperature dependence of the AA interaction energy. Both show that the AA interaction energy increases with temperature at all loadings. The number of neighbor AA interactions decreases with rising temperature, which is energetically less favorable. Hence we see an increase in the AP interaction energy with increasing temperature. It should be noted that the AA interaction energy curves for all temperatures have the same intercept, zero. We expect this trend because there are no AA interactions at infinite dilution.

The qualitative agreement of the AA interaction energy established by our theory with the simulations is welcome because it has provided a much needed platform to understand the adsorbate−adsorbate clustering within sites and between neighboring sites using intrasite and intersite partition functions.

We report an overall error of 47% for the AA interaction energy. The error between the theory and simulations is more pronounced at high loadings. We suspect that the confined geometry of our lattice model, as against the continuum space assumed by simulation, is the prime cause for the inaccurate predictions at high loadings. Fluid crowding forces the adsorbates to sit slightly outside of the lattice sites, which violates our strict lattice assumption. However, one needs to realize that the AA interaction energy contributes only a small fraction of the total energy. The major contributor to the total energy, that is, the AP interaction energy, has been modeled with relatively high accuracy.

Figure 5 plots the total interaction energy as a function of loading and temperature. It should be noted that the total energy, U_{TOT}, is merely a sum of the AP interaction energy, U_{AP}, the AA interaction energy, U_{AA}, and the kinetic energy of motion. The plot reveals that the theory is in good overall consent with the simulations. We observe the correct density and temperature dependence of the total energy. Both theory and simulations show that at all temperatures, the total energy decreases

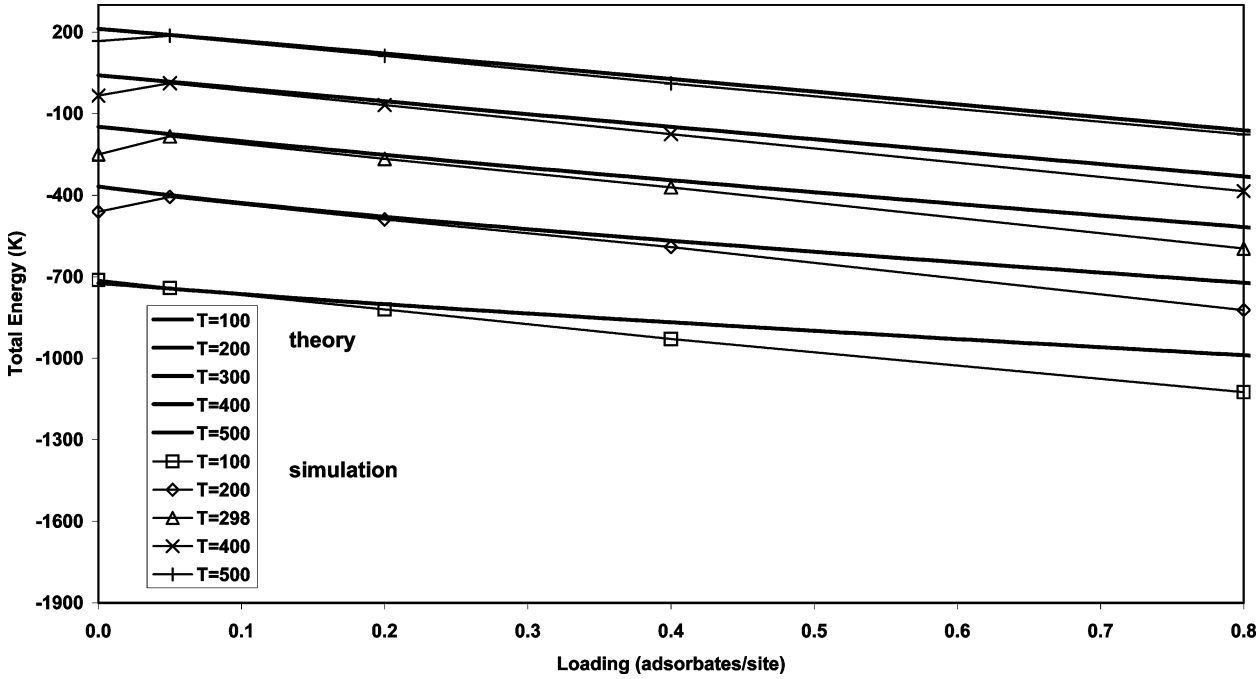

Figure 5. Total energy as a function of fractional occupancy.

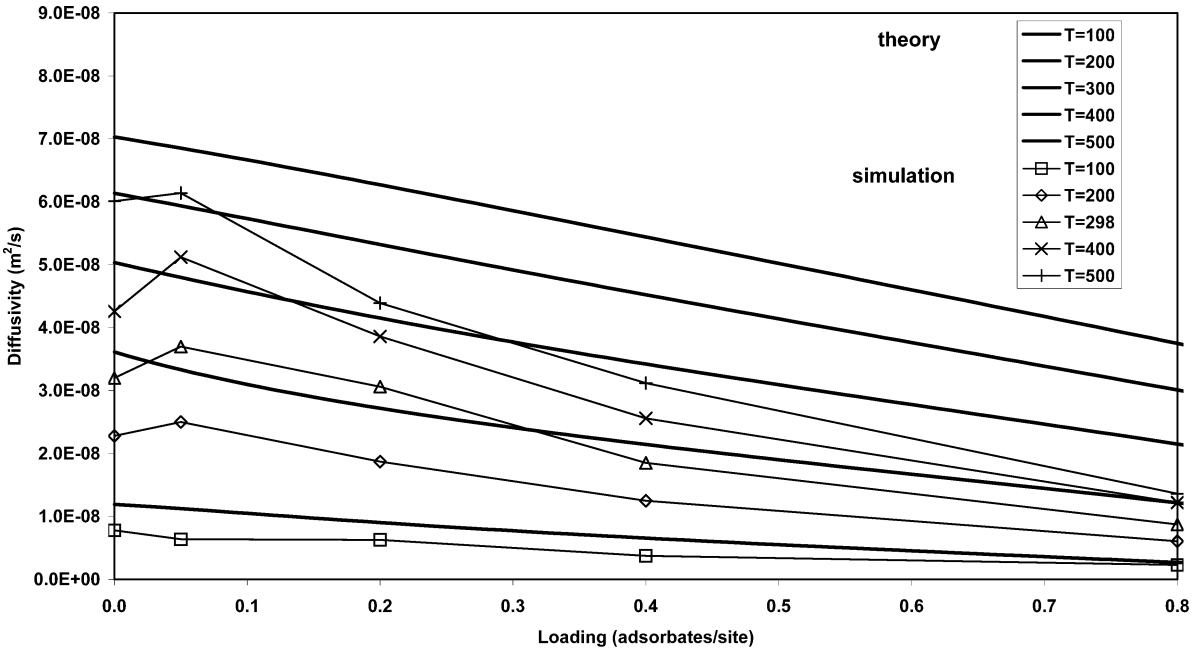

Figure 6. Diffusion coefficient as a function of fractional occupancy.

asloading increases. Also, the total energy increases with temperature at all loadings. Both the density and temperature behavior of the total energy were expected because similar trends were observed in general for U_{AP} and U_{AA}. Quantitatively, the results predicted by the theory are off within an average error of 4.5%. It should be noted that the two errors that were discussed in the plots for U_{AP} and U_{AA} are reflected in the present plot too. For one, our lattice adsorption theory does not predict the maximum in the total energy as shown by simulations, at infinite dilution for higher temperatures. This maximum corresponds to the maximum seen in Figure 2 for U_{AP}. Also, as discussed for U_{AA}, the theory does not follow the simulations at high loadings. The fluid crowding observed by simulations at high loadings is not captured by the theory. However, it should be noted that the fact that U_{AA} constitutes only a fraction of the total energy makes the error less profound than was seen in Figure 4.

From the discussion of Figures 2, 4, and 5, we demonstrated the capabilities of our lattice adsorption theory in successfully capturing the trends shown by simulations. The CH_4-CH_4 interactions and CH_4-O interactions, in other words, the AA interactions and the AP interactions, at different temperatures and loadings are elucidated by exploring the domain of intrasite and intersite partition functions. We noticed that there were two issues that were not handled well by the lattice adsorption theory: (1) infinite dilution adsorbate−pore interaction energy and (2) high-density adsorbate−adsorbate interaction energy. However, we believe that the simplicity and the fundamental basis of this lattice model definitely provide the impetus to carry out further explorations in this area soon.

In Figure 6, we compare the self-diffusion coefficients predicted by our lattice diffusion theory and simulations for methane in Na-Y. It is worthwhile to mention here that the diffusion component of our lattice theory makes use of the results of the lattice adsorption theory. The diffusion component of our lattice theory is explained in section 2 and in ref 2. Unlike the lattice adsorption theory, which incorporated adjustable fitting parameters, our lattice diffusion theory contains absolutely no fitting parameters.

We plot the diffusivity as a function of loading for five temperatures. The lattice diffusivity versus loading profile shares features predicted by the MD simulations. The theory and simulations are in good agreement. We observe the correct temperature and density dependence. Both theory and simulation predict that at all temperatures, the diffusion coefficient decreases with increase in loading. As the loading increases, there are less vacant sites to facilitate diffusive motion through the lattice, the entropic effect, which decreases the diffusivity.

Furthermore, the diffusivity increases with temperature at all loadings. This is expected from the Arrhenius temperature dependence of the diffusivity. At higher temperatures, the molecules attempt more successful "jumps" between sites, which increases the diffusivity.

We notice that the diffusivity predicted by the theory is much higher than the simulations at high loadings. In our recently published paper on the lattice diffusion theory, we mentioned that the theory needs to incorporate the percolative effects of the lattice, which would lower the mean diffusivity, D, at high loadings.[2] We intend to include the percolative behavior soon. We expect the trends shown here to persist, albeit weighted by the percolative effect of the lattice.

The theory is in poor quantitative agreement with the simulations. The theory is off with an average error of 62.9%. Incorporating fitting parameters into the diffusion component of our theory could mask this error. While the inclusion of the adjustable parameters in our lattice diffusion model may enable better quantitative agreement with the simulations, the power of the modeling approach presented here lies in its conceptual simplicity and its ability to compare *reasonably* well with the simulation data on a wide variety of zeolites, which, for one, is demonstrated here with Na-Y.

5. Conclusions

In this work, we have presented a validation analysis of our previously published analytical theories for adsorption and diffusion in nanoporous materials. The results predicted by our theory are tested with MD simulations for the system methane in Na-Y. A very good agreement is found between the theory and simulations. The theory incorporates the atomistic structure of the adsorbent and also incorporates the fundamental physical mechanisms that dictate the behavior of methane molecules in zeolite Na-Y.

While the lattice adsorption theory required five fitting parameters, the diffusion component of the theory incorporated no fitting parameters. The theory was found to be computationally efficient, as it took approximately only a minute to generate the results against 200 h of CPU time required by simulations.

We are currently in the midst of addressing some issues that were left unresolved by the theory, namely, percolative effects at high loadings and infinite dilution behavior of the adsorbate−pore interactions. Also, we are extending our theory for multicomponent fluids.

Notations

symbol	description	units
A	Helmholtz free energy	K/molecule
c_{ij}	number of sites of type j connected to a site of type i	
$D(N,M,T)$	diffusivity as a function of N, M, and T	m^2/s
$D_{0,ij}(x)$	prefactor to diffusivity	m^2/s
$D_{s,eff,i}(x)$	effective diameter of a site as a function of x	Å
E	total energy	K/molecule
$g(N,M)$	configurational degeneracy of the lattice	
$h_{ij}(x,y,T)$	weighting factor to diffusivity	
k	Boltzmann constant	J/mol/K
$\underline{l}$	matrix of distances between sites	Å
m_a	mass of an adsorbate	kg
$m_{s,i}$	maximum occupancy of sites of type i	
M_i	number of sites of type 1	
$n_{s,i}(x)$	number of sites of type $i$with an occupancy of x	
$n\mu$	label of unknowns	
N	number of adsorbates	
$N_{ij,xy}$	number of neighbors between sites of type i with occupancy x and sites of type j with occupancy y	
$q_i(x,T)$	intrasite partition function of sites of type i	
$Q(N,M,T)$	partition function as a function of N, M, and T	
r	Lennard-Jones distance between molecules	Å
r_{min}	distance of well minimum	Å
S	entropy	K/molecule
T	temperature	K
$U_{AP,i}(r,x,T)$	potential energy of a site of type i as a function of radius, occupancy, and temperature	K/molecule
U_{AA}	adsorbate−adsorbate interaction energy	K/molecule
U_{TOT}	total energy	K/molecule
v	velocity of a molecule	m/s
V_A	volume of adsorbate	$Å^3$
$V_{S,i}$	volume of sites of type i	$Å^3$
$\underline{\underline{\mathbf{w}}}_x$	matrix of adsorbate−adsorbate potential energy due to adsorbates in neighboring sites	K
x	occupancy of a site of type i	
y	occupancy of a site of type j	
$\Delta E_{ij}^*(x,y,T)$	difference in total energy between site of type i with site of type j as a function of occupancies x, y, and T	K
θ	fractional occupancy	
δ_{xy}	Kronecker delta function	
μ	chemical potential	K/molecule
ω	angular velocity	rad/s

References and Notes

(1) Kamat, M.; Keffer, D. Generalizing the Quasi-Chemical Lattice Theory to Describe Adsorption in Crystalline Nanoporous Materials. *Mol. Phys.* **2002**, *100*, 2689−2701.

(2) Kamat, M.; Keffer, D. An analytical theory for diffusion of fluids in crystalline nanoporous materials. *Mol. Phys.* **2003**, *101* (10), 1399−1412.

(3) Keffer, D.; Davis, H. T.; McCormick, A. V. The effect of nanopore shape and loading on adsorption selectivity of a binary mixture. *J. Phys. Chem.* **1996**, *100*, 638−645.

(4) Keffer, D.; Davis, H. T.; McCormick, A. V. The effect of nanopore shape on the structure and isotherms of adsorbed fluids. *Adsorption* **1996**, *2*, 9−21.

(5) Keffer, D. Molecular Models of Adsorption and Diffusion in Nanoporous Materials. Ph.D. Thesis, University of Minnesota, July, 1996.

(6) Keffer, D.; McCormick, A. V.; Davis, H. T. Uni-directional and single-file diffusion in $AlPO_4$-5: a molecular dynamics study. *Mol. Phys.* **1996**, *87*, 367−387.

(7) Keffer, D.; McCormick, A. V.; Davis, H. T. Agreement between Theory and Simulation of Single-file diffusion in a molecular sieve.

Proceedings from the XI International Workshop on Condensed Matter Theories; Caracas, Venezuela, June, 1995.

(8) Hahn, K.; Kärger, J. Molecular Dynamics Simulations of Single-File Systems. *J. Phys. Chem.* **1996**, *100*, 316−326.

(9) Keffer, D.; McCormick, A. V.; Davis, H. T. Diffusion and Percolation on Zeolite Sorption Lattices. *J. Phys. Chem.* **1996**, *100*, 967−973.

(10) Kono, H.; Takasaka, A. Statistical mechanics calculation of the sorption characteristics of Ar and N2 in dehydrated zeolite 4A by a Monte Carlo method for determining configuration integrals. *J. Phys. Chem.* **1987**, *91*, 4044−4055.

(11) Razmus, D. M.; Hall, C. K. Prediction of gas adsorption in 5A zeolites using Monte Carlo simulations. *AIChE J.* **1991**, *37*, 769−779.

(12) Van Tassel, P. R.; Davis, H. T.; McCormick, A. V. Monte Carlo calculations of adsorbate placement and thermodynamics in a micropore: Xe in NaA. *Mol. Phys.* **1991**, *73*, 1107−1125.

(13) Van Tassel, P. R.; Davis, H. T.; McCormick, A. V. Monte Carlo calculations Xe arrangement and energetics in the NaA alpha cage. *Mol. Phys.* **1992**, *76*, 411−432.

(14) Van Tassel,, P. R.; Phillips, J. C.; Davis, H. T.; McCormick, A. V. Zeolite adsorption site location and shape shown by simulated isodensity surfaces. *J. Mol. Graphics* **1993**, *11*, 180−184, 188.

(15) Van Tassel, P. R.; Davis, H. T.; McCormick, A. V. Open-system Monte Carlo simulations of Xe in NaA. *J. Chem. Phys.* **1993**, *98*, 8919−8928.

(16) Van Tassel, P. R.; Somers, S. A.; Davis, H. T.; McCormick, A. V. Lattice model and simulation of dynamics of adsorbate motion in zeolites. *Chem. Eng. Sci.* **1994**, *49*, 2979−2989.

(17) Van Tassel, P. R.; Davis, H. T.; McCormick, A. V. New lattice model for adsorption of small molecules and their mixtures in a zeolite micropore. *AIChE J.* **1994**, *40*, 925−934.

(18) Van Tassel, P. R.; Davis, H. T.; McCormick, A. V. Adsorption simulations of small molecules and their mixtures in a zeolite micropore. *Langmuir* **1994**, *10*, 1257−1267.

(19) Soto, J. L.; Myers, A. L. Monte Carlo studies of adsorption in molecular sieves. *Mol. Phys.* **1981**, *42*, 971−983.

(20) Woods, G. B.; Panagiotopolous, A. Z.; Rowlinson, J. S. Adsorption of Fluids in Model Zeolites. *Mol. Phys.* **1988**, *63*, 49−63.

(21) Woods, G. B.; Rowlinson, J. S. Computer Simulations of fluids in zeolites X and Y. *J. Chem. Soc., Faraday Trans. 2* **1989**, *85*, 765−781.

(22) Yashonath, S.; Thomas, J. M.; Novak, A. K.; Cheetham, A. K. The siting, energetics and mobility of saturated hydrocarbons inside zeolitic cages: methane in zeolite Y. *Nature* **1988**, *331*, 601−604.

(23) Yashonath, S.; Demontis, P.; Klein, M. L. A molecular dynamics study of methane in zeolite NaY. *Chem. Phys. Lett.* **1988**, *153*, 551−556.

(24) Demontis, P.; Yashonath, S.; Klein, M. L. Location and mobility of benzene in sodium-Y zeolite by molecular dynamics calculations. *J. Phys. Chem.* **1989**, *93*, 5016−5019.

(25) Yashonath, S. A molecular dynamics study of cage-to-cage migration in sodium Y zeolite: Role of surface-mediated diffusion. *J. Phys. Chem.* **1991**, *95*, 5877−5881.

(26) Yashonath, S.; Demontis, P.; Klein, M. L. Temperature and concentration dependence of adsorption properties of methane in NaY: A molecular dynamics study. *J. Phys. Chem.* **1991**, *95*, 5881−5889.

(27) Santikary, P.; Yashonath, S.; Ananthakrishna, G. A molecular dynamics study of xenon sorbed in sodium Y zeolite. 1. Temperature and concentration dependence. *J. Phys. Chem.* **1992**, *96*, 10469−10477.

(28) Yashonath, S.; Santikary, P. Xenon in sodium Y zeolite 2. Arrhenius relation, mechanism, and barrier height distribution for cage-to-cage diffusion. *J. Phys. Chem.* **1993**, *97*, 3849−3857.

(29) Yashonath, S.; Santikary, P. Diffusion of sorbates in zeolites Y and A: Novel dependence on sorbate size and strength of sorbate−zeolite interaction. *J. Phys. Chem.* **1994**, *98*, 6368−6376.

(30) Klein, H.; Kirschhock, C.; Fuess, H. Adsorption and diffusion of aromatic hydrocarbons in zeolite Y by molecular mechanics calculation and X-ray powder diffraction. *J. Phys. Chem.* **1994**, *98*, 12345−12360.

(31) Gupta, V.; Davis, H. T.; McCormick, A. V. Comparison of the ^{129}Xe NMR chemical shift with simulation in zeolite Y. *J. Phys. Chem.* **1996**, *100*, 9824−9833.

(32) Gupta, V.; Davis, H. T.; McCormick, A. V. ^{129}Xe NMR chemical shifts in zeolites: Effect of Loading studied by Monte Carlo simulations. *J. Phys. Chem.* **1997**, *101*, 129−137.

(33) Keffer, D.; Gupta, V.; Kim, D.; Lenz, E.; Davis, H. T.; McCormick, A. V. A compendium of zeolite potential energy maps. *J. Mol. Graphics* **1996**, *14*, 108−116, 100−104.

(34) Nivarthi, S. S.; Van Tassel, P. R.; Davis, H. T.; McCormick, A. V. Adsorption and energetics of xenon in mordenite: a Monte Carlo simulation study. *J. Chem. Phys.* **1995**, *103*, 3029−3037.

(35) Vernov, A. V.; Steele, W. A. Sorption of xenon in zeolite Rho: A thermodynamics/simulation study. *J. Phys. Chem.* **1993**, *97*, 7660−7664.

(36) Loriso, A.; Bojan, M. J.; Vernov, A.; Steele, W. A. Computer simulation studies of ordered structures formed by rare gases sorbed in zeolite Rho. *J. Phys. Chem.* **1993**, *97*, 7665−7671.

(37) Snurr, R. Q.; June, R. L.; Bell, A. T.; Theodorou, D. N. Molecular simulations of methane adsorption in silicalite. *Mol. Simul.* **1991**, *8*, 73−92.

(38) Snurr, R. Q.; June, R. L.; Bell, A. T.; Theodorou, D. N. A hierarchical atomistic/lattice simulation approach for the prediction of adsorption thermodynamics of benzene in silicalite. *J. Phys. Chem.* **1994**, *98*, 5111−5119.

(39) Demontis, P.; Fois, E. S.; Suffriti, G. B.; Quartieri, S. Molecular dynamics studies on zeolites 4. Diffusion of methane in silicalite. *J. Phys. Chem.* **1990**, *94*, 4329−4334.

(40) Demontis, P.; Suffriti, G. B.; Fois, E. S.; Quartieri, S. Molecular dynamics studies on zeolites 6. Temperature dependence of diffusion of methane in silicalite. *J. Phys. Chem.* **1992**, *96*, 1482−1490.

(41) Nowak, A. K.; Cheetham, A. K.; Pickett, S. D.; Ramdas, S. A computer simulation of the adsorption and diffusion of benzene and toluene in the zeolites Theta-1 and silicalite. *Mol. Simul.* **1987**, *1*, 67−77.

(42) Vigne-Maeder, F.; Jobic H. Adsorption sites and packing of benzene in silicalite. *Chem. Phys. Lett.* **1990**, *169*, 31−35.

(43) Vigne-Maeder, F.; Auroux, A. Potential maps of methane, water, and methanol in silicalite. *J. Phys. Chem.* **1990**, *94*, 316−322.

(44) June, R. L.; Bell, A. T.; Theodorou, D. N. Molecular Dynamics studies of methane and xenon in silicalite. *J. Phys. Chem.* **1990**, *94*, 8232−8240.

(45) June, R. L.; Bell, A. T.; Theodorou, D. N. Transition-state studies of xenon and SF_6 diffusion in silicalite. *J. Phys. Chem.* **1991**, *95*, 8866−8878.

(46) Goodbody, S. J.; Watanabe, K.; MacGowan, D.; Walton, J. P. R. B.; Quirke, N. Molecular simulation of methane and butane in silicalite. *J. Chem. Soc., Faraday Trans.* **1991**, *87*, 1951−1958.

(47) June, R. L.; Bell, A. T.; Theodorou, D. N. Molecular Dynamics studies of butane and hexane in silicalite. *J. Phys. Chem.* **1992**, *96*, 1051−1060.

(48) Snurr, R. Q.; Bell, A. T.; Theodorou, D. N. Prediction of adsorption of aromatic hydrocarbons in silicalite from grand canonical Monte Carlo simulations with biased insertions. *J. Phys. Chem.* **1993**, *97*, 13472−13752.

(49) Nicholas, J. B.; Trouw, F. R.; Mertz, J. E.; Iton, L. E.; Hopfinger, A. J. Molecular Dynamics simulation of propane and methane in silicalite. *J. Phys. Chem.* **1993**, *97*, 4149−4163.

(50) Vigne-Maeder, F. Analysis of ^{129}Xe chemical shifts in zeolites from molecular dynamics calculations. *J. Phys. Chem.* **1994**, *98*, 4666−4672.

(51) Smit, B.; Siepmann, J. I. Computer simulations of the energetics and siting of *n*-alkanes in zeolites. *J. Phys. Chem.* **1994**, *98*, 8442−8452.

(52) Smit, B.; Maesen, T. L. M. Commensurate 'freezing' of alkanes in the channels of a zeolite. *Nature* **1995**, *374*, 42−44.

(53) Bandopadhyay, S.; Yashonath, S. Diffusion anomaly in silicalite and VPI-5 from molecular dynamics simulations. *J. Phys. Chem.* **1995**, *99*, 4286−4292.

(54) Yashonath, S.; Bandopadhyay, S. Surprising diffusion behavior in the restricted regions of silicalite. *Chem. Phys. Lett.* **1994**, *228*, 284−288.

(55) Heffelfinger, G. S.; Pohl, P. I.; Frink, L. J. D. Molecular Dynamics computer simulations of diffusion in porous silicates. *Mater. Res. Soc. Symp. Proc.* **1995**, *366*, 225−230.

(56) Antonchenko, V. Y.; Ilyin, V. V.; Makovsky, N. N.; Khryapa, V. M. Short-range order in cylindrical liquid-filled micropores. *Mol. Phys.* **1988**, *65*, 1171−1183.

(57) Bratko, D.; Blum, L.; Wertheim, M. S. Structure of hard sphere fluids in narrow cylindrical pores. *J. Chem. Phys.* **1989**, *90*, 2752−2757.

(58) Carigan, Y. P.; Vladimiroff, T.; Macpherson, A. K. Molecular Dynamics of hard spheres III. Hard spheres in an almost spherical container. *J. Chem. Phys.* **1988**, *88*, 4448−4450.

(59) Demi, T. Molecular Dynamics studies of adsorption and transport in micropores of different geometries. *J. Chem. Phys.* **1991**, *95*, 9242−9247.

(60) Dunne, J.; Myers, A. L. Adsorption of gas mixtures in micropores: effect of difference in size of adsorbate molecules. *Chem. Eng. Sci.* **1994**, *49*, 2941−2951.

(61) Glandt, E. D. Density distribution of hard-spherical molecules inside small pores of various shapes. *J. Colloid Interface Sci.* **1980**, *77*, 512−524.

(62) Groot, R. D.; Faber, N. M.; van der Eerden, Hard sphere fluids near a hard wall and a hard cylinder. *Mol. Phys.* **1987**, *62*, 861−874.

(63) Han, K. K.; Cushman, J. H.; Diestler, D. J. Grand Canonical Monte Carlo simulations of a Stockmayer fluid in a slit micropore. *Mol. Phys.* **1993**, *79*, 537−545.

(64) Heinbuch, U.; Fischer, J. Liquid argon in a cylindrical carbon pore: molecular dynamics and Born-Green-Yvon Results. *Chem. Phys. Lett.* **1987**, *135*, 587−590.

(65) Jiang, S.; Rhykerd, C. I.; Gubbins, K. E. Layering, freezing transitions, capillary condensation, and diffusion of methane in slit carbon pores. *Mol. Phys.* **1993**, *79*, 373−391.

(66) Macelroy, J. M. D.; Suh, S. H. Computer simulation of moderately dense hard-sphere fluids and mixtures in microcapillaries. *Mol. Phys.* **1987**, *60*, 475−501.

(67) Macelroy, J. M. D.; Suh, S. H. Simulation studies of a Lennard-Jones liquid in micropores. *Mol. Simul.* **1989**, *2*, 313−315.

(68) Macpherson, A. K.; Carignan, Vladimiroff, T. Molecular dynamics of hard spheres II. Hard spheres in a spherical cavity. *J. Chem. Phys.* **1987**, *87*, 1768−1770.

(69) Murad, S.; Ravi, P.; Powles, J. G. A computer simulation study of fluids in model slit, tubular, and cubic micropores. *J. Chem. Phys.* **1993**, *98*, 9771−9781.

(70) Peterson, B. K.; Walton, J. P. R. B.; Gubbins, K. E. Fluid behaviour in narrow pores. *J. Chem. Soc., Faraday Trans. 2* **1986**, *82*, 1789−1800.

(71) Peterson, B. K.; Gubbins, K. E. Phase Transitions in a cylindrical pore: Grand canonical Monte Carlo, mean field theory, and the Kelvin equation. *Mol. Phys.* **1987**, *62*, 215−226.

(72) Saito, A.; Foley, H. C. Curvature and parametric sensitivity in models for adsorption in micropores. *AIChE J.* **1990**, *37*, 429−436.

(73) Sarman, S. The influence of the fluid-wall interaction potential on the structure of a simple fluid in a narrow slit. *J. Chem. Phys.* **1990**, *92*, 4447−4455.

(74) Schoen, M.; Rhykerd, C. L.; Cushman, J. H.; Diestler, D. J. Slit-pore sorption isotherms by the grand-canonical Monte Carlo method: Manifestations of Hysteresis. *Mol. Phys.* **1989**, *66*, 1171−1187.

(75) Somers, S. A.; Davis, H. T. Microscopic dynamics of fluids confined between smooth and atomically structured solid surfaces. *J. Chem. Phys.* **1992**, *96*, 5389−5407.

(76) Somers, S. A.; McCormick, A. V.; Davis, H. T. Superselectivity and solvation forces of a two component fluid adsorbed in nanopores. *J. Chem. Phys.* **1993**, *99*, 9890−9898.

(77) Tan, Z.; Gubbins, K. E. Selective adsorption of simple mixtures in slit pores: A model of methane−ethane mixtures in carbon. *J. Phys. Chem.* **1992**, *96*, 845−854.

(78) Walton, J. P. R. B.; Quirke, N. Capillary condensation: a molecular simulation study. *Mol. Simul.* **1989**, *2*, 361−391.

(79) Page, K. S.; Monson, P. A. Phase equilibrium in a molecular model of a fluid confined in a disordered porous material. *Phys. Rev. E* **1996**, *54*, R29−32.

(80) Vuong, T.; Monson, P. A. Monte Carlo calculations of heats of adsorption in heterogeneous solids. *Langmuir* **1996**, *12*, 5425−5432.

(81) Fan, Y.; Finn, J. E.; Monson, P. A. A Monte Carlo simulation study of adsorption from a liquid mixture at states near liquid−liquid coexistence. *J. Chem. Phys.* **1993**, *99*, 8238−8243.

(82) Peterson, B. K.; Heffelfinger, G. S.; Gubbins, K. E.; Van Swol, F. Layering transitions in cylindrical nanopores. *J. Chem. Phys.* **1990**, *93*, 679−685.

(83) Heffelfinger, G. S.; Van Swol, F.; Gubbins, K. E. Liquid−Vapor coexistence in a cylindrical pore. *Mol. Phys.* **1987**, *61*, 1381−1390.

(84) Demontis, P.; Suffritti, G. B. Molecular Dynamics Investigations of the Diffusion of Methane in a Cubic Symmetry Zeolite of Type ZK4. *Chem. Phys. Lett.* **1994**, *223*, 355.

(85) Beezus, A. G.; Kiselev, A. V.; Lopatkin, A. A.; Pham Quang Du Molecular statistical calculation of the thermodynamic adsorption characteristics of zeolites using the atom−atom approximation. Adsorption of methane by zeolite NaX. *J. Chem. Soc., Faraday Trans.* **1978**, *74*, 367−379.

(86) Coppens, M.-O.; Bell, A. T.; Chakraborty, A. K. Effect of topology and molecular occupancy on self-diffusion in lattice models of zeolites-Monte Carlo simulations. *Chem. Eng. Sci.* **1998**, *53*, 2053−2061.

(87) Auerbach, S. M. Analytical theory of benzene diffusion in Na-Y zeolite. *J. Chem. Phys.* **1997**, *106*, 7810−7815.

(88) Saravanan, C.; Auerbach, S. M. Modeling the concentration dependence of diffusion in zeolites. I. Analytical theory of benzene in Na-Y. *J. Chem. Phys.* **1997**, *107*, 8120−8131.

(89) Saravanan, C.; Auerbach, S. M. Modeling the concentration dependence of diffusion in zeolites. II. Kinetic Monte Carlo simulations of benzene in Na-Y. *J. Chem. Phys.* **1997**, *107*, 8132−8137.

(90) Saravanan, C.; Jousse, F.; Auerbach, S. M. Modeling the concentration dependence of diffusion in zeolites. III. Testing Mean Field Theory for benzene in Na-Y with simulation. *J. Chem. Phys.* **1998**, *108*, 2162−2169.

(91) Weitkamp, J. In *Catalysis and adsorption by zeolites*; Olhmann, G., Vendrine, J. C., Jacobs, P. A., Eds.; Elsevier: Amsterdam, 1991.

(92) Newsam, J. M. In *Zeolites, in solid-state chemistry: Compounds*; Cheetham, A. K., Day, P., Eds.; Oxford University Press: Oxford, U.K., 1992; pp 234−280.

(93) Sanborn, M. J.; Snurr, R. Q. Diffusion of binary mixtures of CF sub 4 and *n*-alkanes in faujasite. *Sep. Purif. Technol.* **2000**, *20*, 1−13.

(94) Eagen, J. A.; Anderson, R. B. Kinetics and equilibrium of adsorption on 4A zeolite. *J. Colloid Interface Sci.* **1975**, *50*, 419.

(95) Karger, J.; Ruthven, D. M. *Diffusion in zeolites and other microporous solids*; Wiley-Interscience: New York, 1992.

(96) Hill, T. L. *Introduction to statistical thermodynamics*; Addison-Wesley Pub. Co.: Reading, MA, 1960.

(97) Allen, M. P.; Tildesely, D. J. *Computer simulation of liquids*; Clarendon Press: Oxford, U.K., 1987.

(98) Haile, J. M. *Molecular dynamics simulation*; John Wiley & Sons: New York, 1992.

(99) Hirschfelder, J. O.; Curtiss, C. F.; Bird, R. B. *Molecular theory of gases and liquids*; Wiley: New York, 1964.

(100) Gear, C. W. *The Numerical Integration of Ordinary Differential Equations of Various Orders*; Report ANL-7126; Argonne National Laboratory: 1966.

(101) Gear, C. W. *Numerical Initial Value Problems in Ordinary Differential Equations*; Prentice Hall, Inc.: Englewood Cliffs, NJ, 1971.

(102) The Universal Library, Numerical recipes online. http://www.ulib.org/webRoot/Books/Numerical_Recipes.